A Combined LQG and Repetitive Controller for High Performance AFM Scanning

by

Arda AYTEKIN

A Thesis Submitted to the
Graduate School of Engineering
in Partial Fulfillment of the Requirements for
the Degree of

Master of Science
in
Mechanical Engineering

Koc University

January 2013

Koc University

Graduate School of Sciences and Engineering

This is to certify that I have examined this copy of a master's thesis by

Arda AYTEKIN

and have found that it is complete and satisfactory in all respects,

and that any and all revisions required by the final

examining committee have been made.

Committee Members:

_____

Cagatay BASDOGAN, Assoc. Prof. Dr. (Advisor)

_____

Yaman ARKUN, Prof. Dr.

_____

Esref ESKINAT, Prof. Dr.

_____

Hakan TEMELTAS, Prof. Dr.

_____

Mustafa UNEL, Prof. Dr.

Date: _____

ABSTRACT

In order to improve the image quality at high scan speeds in AFM imaging, a combined controller architecture employing a linear quadratic Gaussian (LQG) controller and a repetitive controller (RC) is proposed. To calculate the optimal values of the parameters used in the proposed LQG+RC design minimizing the scan error, a Matlab/SIMULINK model of the whole scan process is developed first and then genetic algorithms are employed on the simulation model. In our design, the LQG controller provides more robustness and better tracking performance than a traditional PI controller used for the same purpose. Moreover, since the profile of a scan line is treated as a disturbance in our approach, the proposed LQG controller handles the large variations in scan profile better than the PI controller. The RC on the other hand extends the controller bandwidth and further improves the tracking performance. Our simulations and the experimental results show that the scan performance of the proposed LQG+RC design is better than that of the PI+RC design implemented in our earlier studies.

Keywords: Atomic force microscopy (AFM), nano scanning, system identification, piezo control, repetitive controller (RC), linear quadratic Gaussian regulator (LQG), genetic algorithms (GA)

ÖZET

Yüksek hızlardaki AKM taramalarında görüntü kalitesini artırmak için, LQG ve tekrarlı kontrolcü (TK) kullanan tümleşik bir yapı önerilmiştir. Önerilen LQG+TK tasarımında kullanılan kontrolcü değişkenlerinin, tarama hatasını en aza indirecek şekilde, en iyi değerlerini hesaplamak için, önce tarama işleminin bir MATLAB/Simulink modeli oluşturulmuş ve sonra bu model üzerinde genetik algoritmalar çalıştırılmıştır. Tasarımımızda kullandığımız LQG kontrolcü geleneksel PI kontrolcüsüne göre daha gürbüzdür ve daha iyi izleme başarımı sağlar. Ayrıca, bizim yaklaşımımızda, her tarama satırının profili sistemi bozucu bir etki olarak kabul edildiği için, önerilen LQG kontrolcüsü tarama profilindeki büyük değişimlerin geleneksel PI kontrolcüsüne göre daha iyi üstesinden gelir. Öte yandan TK, kontrolcü bant genişliğini artırarak izleme başarımını daha da iyileştirir. Simulasyon ve deneysel sonuçlarımız önerilen LQG+TK tasarımının daha önceki çalışmalarımızda kullanılan PI+TK yapısından daha iyi olduğunu gösteriyor.

Anahtar Kelimeler: Atomik kuvvet mikroskobu (AFM), nano tarama, system tanımlama, piezo kontrol, tekrarlı kontrolcü (TK), linear quadratic Gaussian (LQG) kontrolcü, genetik algoritmalar (GA)

ACKNOWLEDGEMENTS

I would like to express my sincere gratitude to my thesis supervisor Assoc. Prof. Cagatay BASDOGAN for his support, valuable criticism and guidance, and endless patience throughout my study. I would also like to thank Prof. Yaman ARKUN, Prof. Esref ESKINAT, Prof. Hakan TEMELTAS and Prof. Mustafa UNEL for their invaluable comments and time in reviewing this thesis as my committee members.

I am thankful to Dr. Serkan NECIPOGLU and Ugur ARIDOGAN for guiding me with their valuable comments, Yunus Emre HAS for introducing me to the AFM setup and being always with me during my hard times, and Enes Selman EGE for his support on the measurement circuit of the AFM setup.

I wish to thank my housemates Serkan KULAH, Gokalp GURSEL, Serkan OZKUL and Daulet IZBASSAROV for the great time we had at Siteler. Moreover, I would also like to thank Serkan KULAH, Gokalp GURSEL, Utku BOZ and Denizhan EDEER for their everlasting patience and support during my desperate moments.

I would like to express my sincere gratitude to Mehmet Ali YATBAZ and Dr. Yusuf “the King” SAHILLIOGLU for their priceless friendship. Likewise, I would not have spent such a great time at Koc University, if I had not known Mehmet Akif YALCINKAYA, Baris CAGLAR, Mustafa Resit HABOGLU, Orkun ONAL and Yusuf AYDIN. I hope we kept in touch with each other all the time.

Ladies! Ayse KUCUKYILMAZ, Ezgi EMGIN, Ayten BILGIN, Derya AYDIN, Melisa GUNES, Kubra GULTEKIN and Hande OREN… I would like to thank you all for your always being supportive of me during this journey.

My lab mates, Berkay YARPUZLU and Mehmet AYYILDIZ: Thank you for being great colleagues! I think I have had the best office experience possible with you two. My special thanks go to Mehmet AYYILDIZ for being my buddy in the sports center, my dietician when I overeat, my motivator and/or instructor in technological stuff and my friend all the time – especially during my desperate moments. I think I have exhausted you a lot!

Last but not least, I wish to express my deepest gratitude to the two angels of my life, Mrs. Ayse Mine AYTEKIN and Mr. Suleyman Sureyya AYTEKIN, for their everlasting support and patience. I would also like to thank all my professors at Istanbul Technical University and Koc University, and Ms. Zinet BAL, who have helped me come to where I stand now. Finally, I thank TUBITAK-BIDEB for financially supporting me during the last year of my M.Sc. studies.

TABLE OF CONTENTS

LIST OF TABLES

LIST OF FIGURES

Chapter 1

INTRODUCTION

Atomic force microscope (AFM) is a widely used tool for surface imaging at nano scale. The main reasons for such a wide use of AFM are the ease of sample preparation, the ability to operate in different environments, and its relatively lower cost. An AFM system mainly consists of a cantilever probe to scan the sample surface, a piezo-actuated stage to place the sample with respect to the probe, and a laser-based system for measuring the vertical displacement of the cantilever probe (see the schematic representation of our AFM system in Figure 1.1). In amplitude-modulated tapping-mode AFM scanning, the probe is initially vibrated sinusoidally at near its resonant frequency in free air (A_{free}). As the sample surface is brought close to the probe by means of the piezo stage, the vibration amplitude of the probe drops due to atomic interactions. The goal in AFM scanning is to keep the amplitude of the probe (A_{act}) at a set value ($A_{act} = A_{set} < A_{free}$) using a feedback-loop, which controls the separation distance between the probe tip and the surface (see Figure 1.1) by commanding the piezo stage. Hence, the dynamic response of the piezo stage as

well as the interaction dynamics between the probe and the surface significantly affect the scan speed and the image quality.

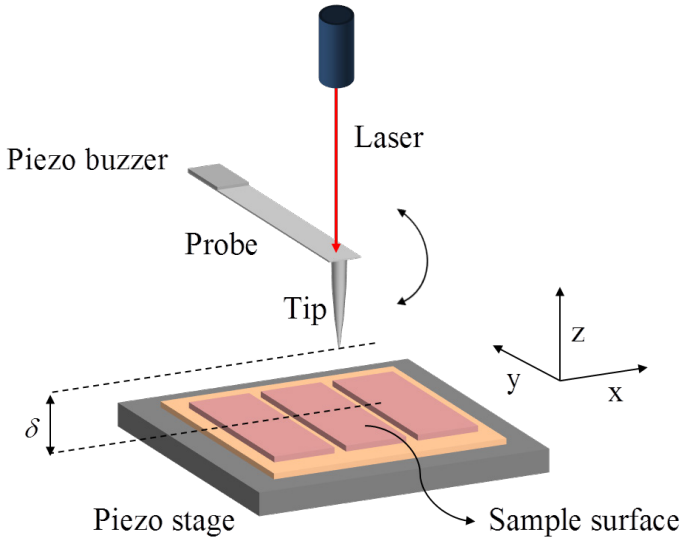

Figure 1.1 Tapping mode AFM: the probe is actuated sinusoidally by a piezo buzzer around its resonant frequency, and the actuation amplitude is measured using a Laser Doppler Vibrometer (LDV). The sample surface is placed on a 3-axis piezo-actuated stage, whose x-axis is given a staircase input; y-axis, a triangular input; and z-axis is controlled to keep the actuation amplitude of the probe at a set value despite the variations in surface profile being scanned.

The dynamic performance of a piezo stage used in an AFM system is influenced by nonlinear effects such as creep and hysteresis, and undesired structural modes at high frequencies, which prevent it from operating extended periods of time for long range motions, and at high scan speeds [1]. Therefore, a great deal of effort has been devoted to address these problems using feedback and/or feedforward controllers (see the reviews in [2, 3]).

Traditionally, PI, PII, and PID feedback controllers are used in AFM systems to regulate the lateral (x- and y-axes) and the perpendicular movements (z-axis) of a piezo stage [4]. However, the control bandwidth achievable by these feedback controllers is limited, and they are incapable of handling high frequency dynamics. Moreover, re-tuning of the controller gains is required when the components of the AFM system change [5].

H_∞ controller is suggested to address the limitations of the traditional feedback controllers. Compared to a PI controller, improvements of forty times in bandwidth [6] and eighteen times in settling time are achieved [7] using an H_∞ controller. In [8], a controller scheme based on two H_∞ controllers in series is also proposed; one is used for performance improvement while the other is used for robustness.

Furthermore, a design employing a feedforward controller in tandem with a feedback controller yields better results than that of feedback-only designs. In [9, 10], a controller structure consisting of a traditional feedback and an inversion-based feedforward controller is proposed. The performance of the feedback-only system, quantified by the tracking error, is improved by over 75% at high scan speeds in [10]. In [11], an H_∞ feedback with an inversion-based feedforward controller is suggested to improve the scan performance at high scan speeds. As an alternative to an inversion-based feedforward controller, various types of learning-based feedforward controllers are also suggested to improve the scan performance in AFM systems. The so-called “Surface Topography Learning Observer” is employed with a traditional feedback controller to reduce the scan

error at high scan speeds [12]. An H_∞ feedback controller is combined with an iterative learning controller (ILC) in [13] and eight times higher scan rates are achieved. [14] suggests that a further improvement in performance can be achieved if a frequency domain delegation is utilized between H_∞ feedback and ILC feedforward controllers. Another learning-based feedforward controller is repetitive controller (RC), which has been also used in tandem with a PI controller [15, 16] and with an H_∞ controller [17] to improve the scan speed in AFM imaging.

In this thesis, we suggest a controller structure which consists of a model-based feedback controller and a learning-based feedforward controller for high performance AFM scanning. A Linear Quadratic Gaussian (LQG) controller is proposed as a full state feedback controller to provide robustness and for set-point tracking. To further improve the tracking performance at high scan speeds, we propose an RC as an add-on feedforward controller. The major contributions of this study can be listed as follows:

1) In our earlier studies, we have combined the RC with a traditional feedback controller (PI) and achieved a performance improvement of up to sevenfold compared to the feedback-only design [16]. The fact that the RC utilizes the profile of the previous scan line while scanning the current line leads to a better scan performance. However, if there is a significant difference between the consecutive scan profiles, the tracking performance of the PI+RC is poor. Our scanning simulations performed with 100 nm steps have shown that when the change in height exceeds 50%, undesired peaks occur in the scan profile [18]. As

a remedy to this problem, we propose the LQG controller for the z-axis positioning the piezo stage. The LQG improves the disturbance rejection capability of our scanner. Since the profile of a scan line is treated as a disturbance in our approach, the proposed LQG controller handles the large variations in scan profile better than the traditional PI controller. Moreover, since LQG is a full state feedback controller, it enables us to further extend the effective bandwidth of the scanner. Compared to H_∞ feedback controller, the proposed LQG controller is less conservative in robustness, and hence can be more aggressive in tracking performance. In our approach, the robustness of the LQG controller against the nonlinearities in the system is investigated for optimal values of control parameters via iterations in a realistic simulation environment. This requires an accurate identification of the system components, which is also accomplished in this study. The most relevant line of research in the context of our study is a recent paper published by Habibullah and Petersen [19]. They use an LQG controller for lateral positioning (x- and y-axes) of the piezo tube actuator utilized in their AFM setup. An internal model of the reference signal is included in the model of the piezo actuator to reduce the steady state tracking error.

2) In most of the earlier studies involving a controller design, the AFM scans have been performed in contact mode. In this mode, the probe does not vibrate and hence the dynamics of interactions between the probe tip and the sample surface has been neglected in the earlier studies. However, in tapping-mode AFM scanning, this dynamics cannot be

neglected and plays a crucial role in scan performance. In fact, we show that the bandwidth of this interaction is narrower than that of the piezo stage, and thus, it is the bottleneck of scan performance. In this regard, the proposed LQG controller, which is an optimal state feedback controller, speeds up both the dynamics of the piezo stage and the interaction between the probe and the surface, simultaneously.

3) We have developed a MATLAB/Simulink model of the whole scan process and then utilized genetic algorithms on the simulation model to calculate the optimal values of the parameters used in the proposed LQG+RC design such that the integral of absolute scan error (IAE) is minimized. The scanning experiments performed in the simulation environment under different conditions using these optimal parameters show an excellent agreement with the ones performed in the physical world using our AFM setup. Hence, the availability of such a simulation model enables us to design a new controller and investigate its performance before conducting physical AFM experiments.

The following chapter introduces the components of our AFM setup. In Chapter 3, we develop transfer function models of our piezo stage and the interaction dynamics between the probe and the surface through system identification. The design and the analysis of the LQG+RC are given in Chapter 4. The scanning experiments and the results are reported in Chapter 5. We discuss our results in Chapter 6 and conclude the study with final remarks in Chapter 7.

Chapter 2

AFM SETUP

In this thesis, an open-architecture AFM system is used to scan nano scale surfaces in tapping mode [16, 20]. This home-made AFM set-up mainly consists of a piezo-actuated probe for scanning, a Laser Doppler Vibrometer (LDV from Polytec GmbH) for measuring the probe's velocity, and a piezo stage for precise positioning of the scanned surface with respect to the probe (Figure 1.1). Sample surfaces to be scanned are placed on the closed-loop 3-axis piezo-actuated stage (P-517.3CD from Physik Instrumente) to be brought in close interaction with the probe. It is equipped with 16-bit resolution capacitive sensors mounted on its x-, y- and z-axes, and has a stroke of 100 μm × 100 μm × 20 μm along those axes. The piezo stage has an internal PI controller to deal with the hysteresis and creep effects, and a Notch Filter to reduce the adverse effects of high frequency dynamics (Figure 2.1). The coefficients of this internal controller and the filter are factory-tuned for optimal performance. The raster scan motion of the stage on the xy-plane is defined by the user while the z-axis motion (z_{act}) is controlled according to the actual vibration amplitude of the probe, A_{act}. The probe (OMCL-AC160TS) is actuated by a piezo buzzer to vibrate

slightly below its resonance frequency (306.7 kHz). The tip velocity of the probe is measured by the LDV. Since the vibration frequency of the probe exceeds the sampling frequency (f_s = 500 Hz) of the control loop, the measured signal is passed through a Root-Mean-Square converter (AD637JDZ from Analog Devices) to detect changes in probe's amplitude.

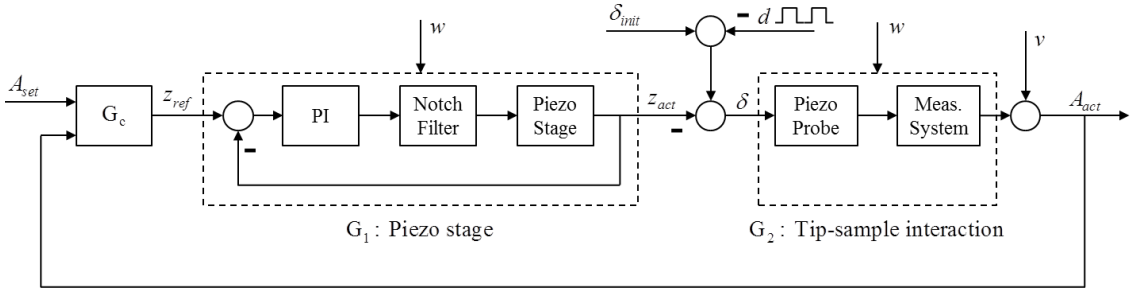

Figure 2.1 The block diagram of our AFM setup.

Initially, the probe vibrates at free air, $A_{act} = A_{free}$, and the sample is placed on the stage at a distance of δ_{init} from the probe. Then, the stage is brought close to the probe until the distance between the probe tip and the surface, δ, becomes small enough and the vibration amplitude of the probe drops to $A_{act} = A_{set} = 0.7 \times A_{free}$. During the raster scanning of a surface, the goal is to keep the amplitude of the probe vibrations at A_{set} by controlling the z-axis movements of the piezo stage. If these movements are recorded, the profile of the scanned surface, d, can be obtained easily (Figure 2.1). In order to design a fast and robust controller, G_c, to regulate the z-axis movements of the piezo stage, transfer function models of the piezo stage, G_1, and the tip-sample interaction, G_2, are required.

Chapter 3

SYSTEM IDENTIFICATION

To obtain the transfer function models of the piezo stage (G_1) and the tip-sample interaction (G_2), two main identification signals are used. The time-dependent responses of G_1 and G_2 are investigated using an amplitude modulated square wave. The frequency dependent responses of the same systems are investigated using a frequency modulated sine wave (i.e. frequency sweep approach).

First, the transfer function models of G_1 and G_2 are written in discrete time in the following form:

$$G(z) = \frac{Y(z)}{U(z)} = \frac{b_m z^m + b_{m-1} z^{m-1} + \ldots + b_0}{z^n + a_{n-1} z^{n-1} + \ldots + a_0}. \quad (3.1)$$

To investigate the time-dependent response of the piezo stage, an amplitude modulated square wave is applied to the stage (see the dashed blue line in Figure 3.1a), and the corresponding displacement (see the dotted red line in Figure 3.1a) is measured through the capacitive sensors in the stage. Then, we formulate the input-output relation in a least squares sense as follows:

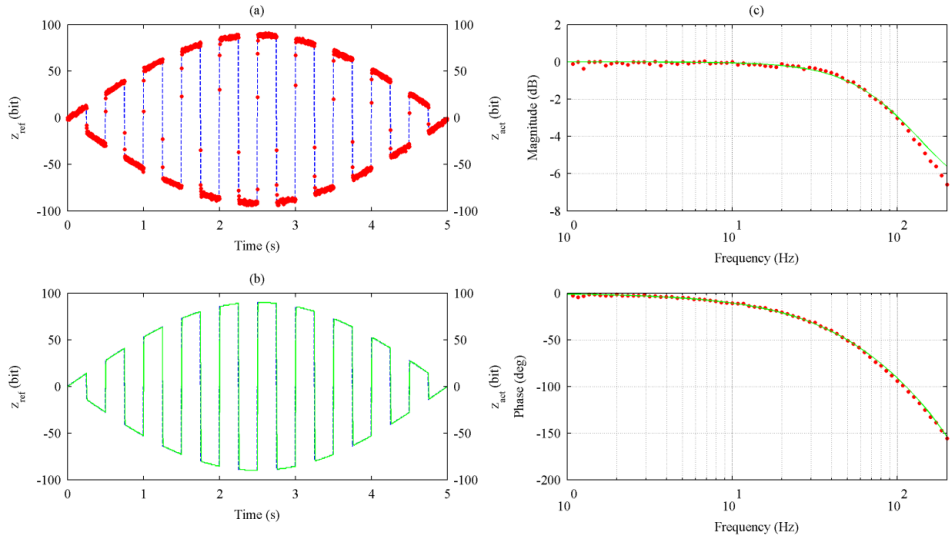

Figure 3.1 The time-dependent response of (a) the piezo stage (dotted red line, plotted with respect to the right vertical axis) and (b) its transfer function model (solid green line, plotted with respect to the right vertical axis) to the amplitude modulated input signal (dashed blue line, plotted with respect to the left vertical axis). (c) The experimental (red dots) and the theoretical (solid green line) Bode plots of the piezo stage.

$$\overbrace{\begin{bmatrix} y_{1+n} \\ \vdots \\ y_{k+n} \\ \vdots \\ y_M \end{bmatrix}}^{\lambda} = \overbrace{\begin{bmatrix} -y_{1+n-1} & \cdots & -y_1 & u_{1+m} & \cdots & u_1 & t_1 \\ \vdots & \ddots & \vdots & \vdots & \ddots & \vdots & \vdots \\ -y_{k+n-1} & \cdots & -y_k & u_{k+m} & \cdots & u_k & t_k \\ \vdots & \ddots & \vdots & \vdots & \ddots & \vdots & \vdots \\ -y_{M-1} & \cdots & -y_{M-n} & u_{M-n+m} & \cdots & u_{M-n} & t_{M-n} \end{bmatrix}}^{\phi} \underbrace{\begin{bmatrix} a_{n-1} \\ \vdots \\ a_0 \\ b_m \\ \vdots \\ b_0 \\ C \end{bmatrix}}_{\theta} + \underbrace{\begin{bmatrix} e_1 \\ \vdots \\ e_k \\ \vdots \\ e_{M-n} \end{bmatrix}}_{\varepsilon}. \qquad (3.2)$$

Here, n and m ($n \geq$ m) represent the number of poles and zeros of the transfer function G_1, respectively, M is the number of observations, λ is the $(M - n) \times 1$ measurement vector, ϕ is the $(M - n) \times (m + n + 2)$ regressor matrix, θ is the $(m + n + 2) \times 1$ coefficient vector, u_k's

are the inputs at time instances k, and ε is the $(M - n) \times 1$ error vector. The coefficient C in vector θ accounts for the creep effects. The coefficient vector is calculated using the pseudo inverse of the regressor matrix as:

$$\theta = \left(\phi^{\mathrm{T}}\phi\right)^{-1}\phi^{\mathrm{T}}\lambda. \tag{3.3}$$

As a result, the following minimum order transfer function is obtained by trial and error for the piezo stage:

$$\mathrm{G}_1(z) = \frac{0.673z^2 - 0.094z - 0.286}{1.001z^3 - 0.476z^2 - 0.363z + 0.131}. \tag{3.4}$$

Figure 3.1b shows the time-dependent response of the stage model (solid green line) for the amplitude modulated input signal (dashed blue line).

To validate this transfer function model, frequency sweep experiments are performed on the stage. For this purpose, a frequency modulated sine wave is applied to the stage and the corresponding displacement is measured through the capacitive sensors in the stage. To obtain the experimental Bode plots of the stage, we plot the magnitude and phase values at discrete frequencies (see the red dots in magnitude and phase diagrams in Figure 3.1c). As shown in the figure, the Bode plots obtained through the transfer function model (solid green lines), G_1, agrees well with the experimental ones.

The same identification procedure is repeated for obtaining the transfer function model, G_2 of the tip-sample interaction (see Figure 2.1). This time, separation distance $\delta = -\Delta z_{act}$ and the vibration amplitude of the probe, A_{act}, are the input to and the output of the

system (Figure 3.2a). Then, the following transfer function model is obtained for the interaction dynamics:

$$G_2(z) = \frac{0.003z - 0.001}{z^2 - 1.199z + 0.212}. \tag{3.5}$$

Figure 3.2b shows the time-dependent response of the interaction model (solid green line) for the amplitude modulated input signal (dashed blue line). In addition, Figure 3.2c compares the experimental Bode plots obtained by the frequency sweep approach with the ones obtained from the transfer function model.

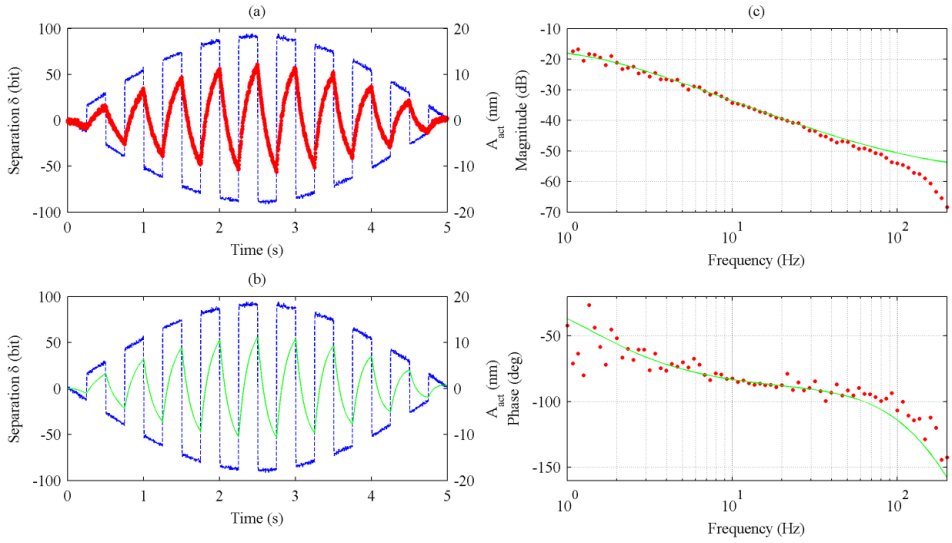

Figure 3.2 The time-dependent response of (a) the tip-sample interaction (dotted red line, plotted with respect to the right vertical axis) and (b) its transfer function model (solid green line, plotted with respect to the right vertical axis) to the amplitude modulated input signal (dashed blue line, plotted with respect to the left vertical axis). (c) The experimental (red dots) and the theoretical (solid green line) Bode plots of the tip-sample interaction.

Chapter 4

CONTROLLER DESIGN

Having derived the transfer function models of the system components, G_1 and G_2, we focus on the controller design G_c, shown in Figure 2.1. Our design consists of an LQG controller (see the dashed green box in Figure 4.1) and an RC (see the dashed red box in Figure 4.1). If the switch (*SW*) shown in Figure 4.1 is open, we have a stand-alone LQG controller, otherwise (*SW* is closed), the proposed controller, LQG+RC, is active.

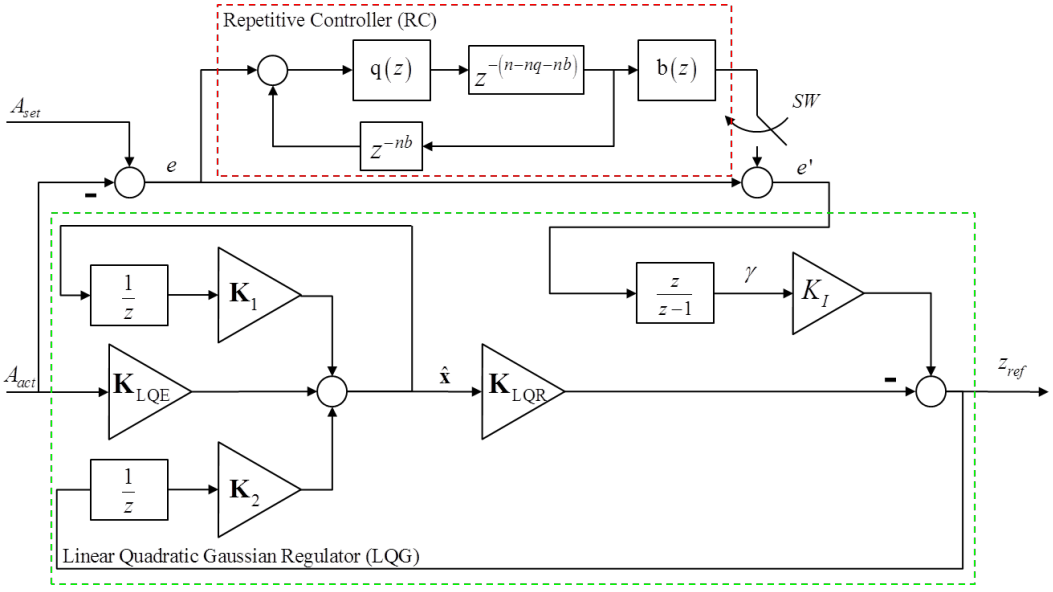

Figure 4.1 The detailed block diagram of the proposed LQG+RC structure.

4.1 Design of the LQG Controller

The LQG controller is simply the combination of a Kalman filter, a linear quadratic estimator (LQE), and a linear quadratic regulator (LQR). Hence, the LQG controller design involves the calculation of the Kalman state observer gain $\mathbf{K}_{\mathrm{LQE}}$ and the state feedback gain $\mathbf{K}_{\mathrm{LQR}}$ (see Figure 4.1). Also, an integral gain, K_I, is used to eliminate the amplitude error ($e = A_{set} - A_{act}$). To design the LQG controller, we first transform the transfer function model of the plant, $G = G_1G_2$, into the augmented state space representation G_{aug}, where the integrated error dynamics is governed by $\gamma_{k+1} = e_{k+1} + \gamma_k$ (see Figure 4.1):

$$
\mathrm{G}_{\mathrm{aug}}:\left[\begin{array}{c}\mathbf{x}_{\mathrm{k}+1}\\ \hline \gamma_{k+1}\end{array}\right]=\overbrace{\left[\begin{array}{c|c}\mathbf{A} & \mathbf{0}\\ \hline -\mathbf{CA} & 1\end{array}\right]}^{\mathbf{A}_{\mathrm{aug}}}\left[\begin{array}{c}\mathbf{x}_{\mathrm{k}}\\ \hline \gamma_k\end{array}\right]+\overbrace{\left[\begin{array}{c}\mathbf{B}\\ \hline -\mathbf{CB}\end{array}\right]}^{\mathbf{B}_{\mathrm{aug}}}u_k+\left[\begin{array}{c}\mathbf{0}\\ \hline 1\end{array}\right]A_{set}+\left[\begin{array}{c}\mathbf{W}\\ \hline 1\end{array}\right]w_k
$$

$$
y_k=\left[\mathbf{C}\;\vdots\;0\right]\left[\begin{array}{c}\mathbf{x}_{\mathrm{k}}\\ \hline \gamma_k\end{array}\right]+v_k,
$$

$$
\mathbf{A}=\begin{bmatrix}1.674 & -0.419 & -0.465 & 0.467 & -0.222\\ 1 & 0 & 0 & 0 & 0\\ 0 & 1 & 0 & 0 & 0\\ 0 & 0 & 0.5 & 0 & 0\\ 0 & 0 & 0 & 0.25 & 0\end{bmatrix}, \tag{4.1}
$$

$$
\mathbf{B}=\begin{bmatrix}0.125 & 0 & 0 & 0 & 0\end{bmatrix}^{\mathrm{T}},\ \mathbf{W}=\begin{bmatrix}1 & 1 & 1 & 1 & 1\end{bmatrix}^{\mathrm{T}},
$$

$$
\mathbf{C}=\begin{bmatrix}0 & 0.018 & -0.01 & -0.014 & 0.025\end{bmatrix}.
$$

Here, $\mathbf{x}_{\mathrm{k}}$ represents the states of the plant, e_k is the amplitude error, u_k is the input to the plant (z_{ref} in Figure 4.1), w_k is the Gaussian state noise, y_k is the output (A_{act} in Figure 4.1), and v_k is the Gaussian measurement noise at time instances k. The matrices **A**, **B** and **C** are

the state, input, and the output matrices of the plant, respectively. The states are assumed to be equally affected by the Gaussian state noise (see the **W** vector in (4.1)). It is straightforward to show that the plant is both controllable and observable (i.e. the controllability and observability matrices are full rank).

Next, we design the LQE based on the standard Kalman filter implementation as follows [21]:

$$
\begin{aligned}
&\mathbf{P}_{\mathrm{k|k-1}} = \mathbf{A}\,\mathbf{P}_{\mathrm{k-1|k-1}}\,\mathbf{A}^{\mathrm{T}} + \mathbf{W}\,R_w\,\mathbf{W}^{\mathrm{T}},\\
&\mathbf{K}_{\mathrm{LQE}} = \mathbf{P}_{\mathrm{k|k-1}}\,\mathbf{A}^{\mathrm{T}}\left(\mathbf{A}\,\mathbf{P}_{\mathrm{k|k-1}}\,\mathbf{A}^{\mathrm{T}} + R_v\right)^{-1},\\
&\hat{\mathbf{x}}_{\mathrm{k|k}} = \underbrace{\left(\mathbf{I} - \mathbf{K}_{\mathrm{LQE}}\mathbf{C}\right)\mathbf{A}}_{\mathbf{K}_1}\hat{\mathbf{x}}_{\mathrm{k-1|k-1}} + \underbrace{\left(\mathbf{I} - \mathbf{K}_{\mathrm{LQE}}\mathbf{C}\right)\mathbf{B}}_{\mathbf{K}_2}u_{k-1} + \mathbf{K}_{\mathrm{LQE}}\,y_k,\\
&\mathbf{P}_{\mathrm{k|k}} = \left(\mathbf{I} - \mathbf{K}_{\mathrm{LQE}}\mathbf{A}\right)\mathbf{P}_{\mathrm{k|k-1}}.
\end{aligned}
\tag{4.2}
$$

Here, $\mathbf{P}_{\mathrm{i|j}}$ represents the variance of the estimation error at time instance *i* based on the information available at time instance *j*, $\hat{\mathbf{x}}_{\mathrm{i|j}}$ is the estimated states at time instance *i* based on the information available at time instance *j*, and **I** is the identity matrix of appropriate size. Also, R_w is the variance of the Gaussian state noise and R_v is the variance of the Gaussian measurement noise, which is measured to be R_v = 0.03 nm in our system. The ratio of R_w / R_v represents the relative importance of modeling uncertainty to the measurement uncertainty and is selected optimally as discussed in Chapter 4.3. The static (i.e. steady state) observer gain $\mathbf{K}_{\mathrm{LQE}}$, and hence the static gains $\mathbf{K}_1$ and $\mathbf{K}_2$ appearing in Figure 4.1 are obtained offline by iteratively solving (4.2) until $\mathbf{P}_{\mathrm{k|k}}$ converges.

To design the LQR, we define the following cost function, J, and solve the related discrete algebraic Riccati equation, which minimizes the cost function [21]:

$$J = \sum_k \left(\begin{bmatrix} \mathbf{x}_k \\ \hline \gamma_k \end{bmatrix}^{\mathrm{T}} \tilde{\mathbf{Q}} \begin{bmatrix} \mathbf{x}_k \\ \hline \gamma_k \end{bmatrix} + u_k^T R\, u_k \right),$$

$$\tilde{\mathbf{Q}} = \left[\begin{array}{ccccc:c} R & 0 & 0 & 0 & 0 & 0 \\ 0 & R & 0 & 0 & 0 & 0 \\ 0 & 0 & R & 0 & 0 & 0 \\ 0 & 0 & 0 & R & 0 & 0 \\ 0 & 0 & 0 & 0 & R & 0 \\ \hdashline 0 & 0 & 0 & 0 & 0 & Q \end{array}\right], \tag{4.3}$$

$$\mathbf{K}_{\mathrm{aug}} = \left[\mathbf{K}_{\mathrm{LQR}} \;\vdots\; K_I \right] = \left(\mathbf{B}_{\mathrm{aug}}^{\mathrm{T}} \mathbf{S}_{\mathrm{k+1}} \mathbf{B}_{\mathrm{aug}} + R \right)^{-1} \left(\mathbf{B}_{\mathrm{aug}}^{\mathrm{T}} \mathbf{S}_{\mathrm{k+1}} \mathbf{A}_{\mathrm{aug}} \right),$$

$$\mathbf{S}_{\mathrm{k}} = \tilde{\mathbf{Q}} + \mathbf{A}_{\mathrm{aug}}^{\mathrm{T}} \left(\mathbf{S}_{\mathrm{k+1}} - \mathbf{S}_{\mathrm{k+1}} \mathbf{B}_{\mathrm{aug}} \left(\mathbf{B}_{\mathrm{aug}}^{\mathrm{T}} \mathbf{S}_{\mathrm{k+1}} \mathbf{B}_{\mathrm{aug}} + R \right)^{-1} \mathbf{B}_{\mathrm{aug}}^{\mathrm{T}} \mathbf{S}_{\mathrm{k+1}} \right) \mathbf{A}_{\mathrm{aug}}$$

where, $\mathbf{S}_{\mathrm{k}}$ is the unique positive definite solution to the discrete algebraic Riccati equation, $\tilde{\mathbf{Q}}$ and R are the weights penalizing the states of the plant augmented by the integrated error, γ_k, and the controller output, respectively. For the finite horizon case, the solution $\mathbf{S}_{\mathrm{k}}$ is obtained by starting from a terminal condition, $\mathbf{S}_{\mathrm{N}}$, and iterating backward in time. For the infinite horizon case (i.e. steady state solution for $\mathrm{N} \rightarrow \infty$), however, the solution $\mathbf{S}_{\mathrm{k}}$ converges to a constant value for any $\mathbf{S}_{\mathrm{N}} \geq \mathbf{0}$ [22]. The ratio of Q / R represents the relative importance of the amplitude error to the controller output and is selected optimally as discussed in Chapter 4.3. The static feedback gain $\mathbf{K}_{\mathrm{aug}}$ is obtained offline by iterating (4.3) until $\mathbf{S}_{\mathrm{k}}$ converges.

4.2 Design of the RC

Our RC is designed based on the regeneration spectrum [16], which is defined as follows:

$$\left| \mathrm{q}(z)\left[1-\mathrm{b}(z)\frac{\mathrm{L}(z)}{1+\mathrm{L}(z)}\right]\right| < 1 \tag{4.4}$$

where, L(z) denotes the loop transfer function of the LQG-regulated plant, and the filters b(z) and q(z) are designed to stabilize the RC. Since (4.4) is a sufficient condition for the stability of the RC, the filter b(z) is selected as simply the inverse of the closed loop system. To reduce the effect of undesired loop gains at high frequencies, the filter q(z) is designed as a low pass filter, as given below:

$$\mathrm{q}(z) = \frac{K_q}{\left(z - e^{-2\pi f_q T_s}\right)^{N_q}} \tag{4.5}$$

where f_q is the cut-off frequency and N_q is the degree of the filter, respectively. The selection of optimal values for the parameters f_q and N_q are discussed in Chapter 4.3. The parameter K_q is adjusted to make the DC gain of the filter unity.

The parameter n in Figure 4.1 represents the number of samples memorized during one repetitive period of an AFM scan (i.e. a back-and-forth movement along the x-axis in Figure 1.1). The parameters *nb* and *nq* in Figure 4.1 denote the sample advances (i.e. phase compensators) and are selected optimally as discussed in Chapter 4.3.

4.3 Optimal Selection of Parameters

The optimal values of the ratios R_w / R_v and Q / R used for the design of the LQG controller, and the parameters nb, nq, f_q, and N_q used for the design of the RC are obtained by the Genetic Algorithms Toolbox of MATLAB. For this purpose, we first construct a MATLAB/Simulink model of the system shown in Figure 2.1. This simulation model consists of the transfer function models of the proposed controller (G_c), the piezo stage (G_1) and the tip-sample interaction (G_2). Moreover, the measurement noise as well as the nonlinear effects such as the saturation on the probe's vibration amplitude, ($0 \leq A_{act} \leq A_{free}$), and integer constraints and rate limits on the output of the piezo stage are also implemented in the simulation model. Then, we simulate scanning steps with a pitch distance of 3 μm and abrupt transitions in height from 100 nm to 500 nm and vice versa as shown in Figure 4.2. Finally, we use this simulation environment within the Genetic Algorithms Toolbox of MATLAB to search for the optimal values of the design parameters such that the integral of absolute error (i.e. $IAE = \int |e(t)| dt$) is minimized.

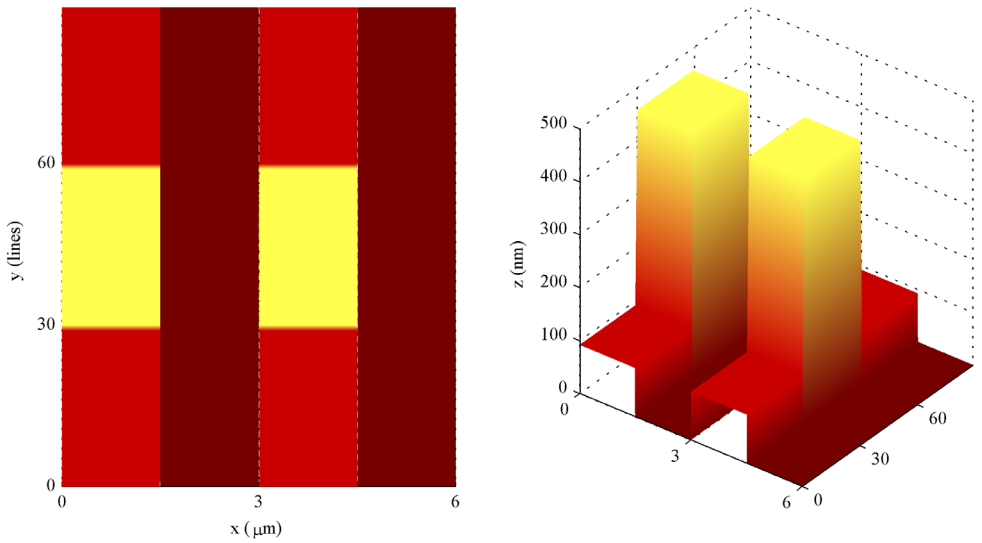

Figure 4.2 The surface profile used in our scan simulations.

The optimal values of the ratios used for the LQG controller are calculated as R_w / $R_v = 6.336 \times 10^6$, and Q / $R = 2.760 \times 10^5$. As a result, the gains, $\mathbf{K}_{\mathrm{LQE}}$, $\mathbf{K}_{\mathrm{LQR}}$, and K_I are obtained as:

$$\begin{aligned} \mathbf{K}_{\mathrm{LQE}} &= \begin{bmatrix} 49.880 & 49.879 & 49.879 & 49.874 & 49.870 \end{bmatrix}^{\mathrm{T}}, \\ \mathbf{K}_{\mathrm{LQR}} &= \begin{bmatrix} 11.216 & -7.117 & -3.372 & 4.354 & -1.447 \end{bmatrix}, \\ K_I &= 225.212 \end{aligned} \tag{4.6}$$

Similarly, the optimal values of the parameters used for the RC are calculated as $nb = 1$, $nq = 5$, $f_q = 77.97$ Hz, and $N_q = 3$. As a result, the transfer function models of the filters, b(z) and q(z), are obtained as:

$$\mathrm{b}(z)=\frac{1.930(z+0.564)(z-0.730)\left(z^2-0.563z+0.183\right)}{(z+0.583)(z-0.724)\left(z^2+0.142z+0.014\right)}$$
$$\mathrm{q}(z)=\frac{0.244}{(z-0.375)^3}. \tag{4.7}$$

4.4 Analysis of the Design

We first investigate the stability of the proposed LQG+RC controller (the stability and performance analysis for the PI+RC has already been given in our earlier publication [16]). For checking the stability of the LQG controller, the pole-zero map of the regulated plant is constructed. As shown in Figure 4.3a, the LQG regulated plant does not have any unstable poles and/or non-minimum phase zeros. The stability of the RC is investigated by the regeneration spectrum (Figure 4.3b). As shown in the figure, the inequality given in (4.4) is satisfied for the frequencies of interest.

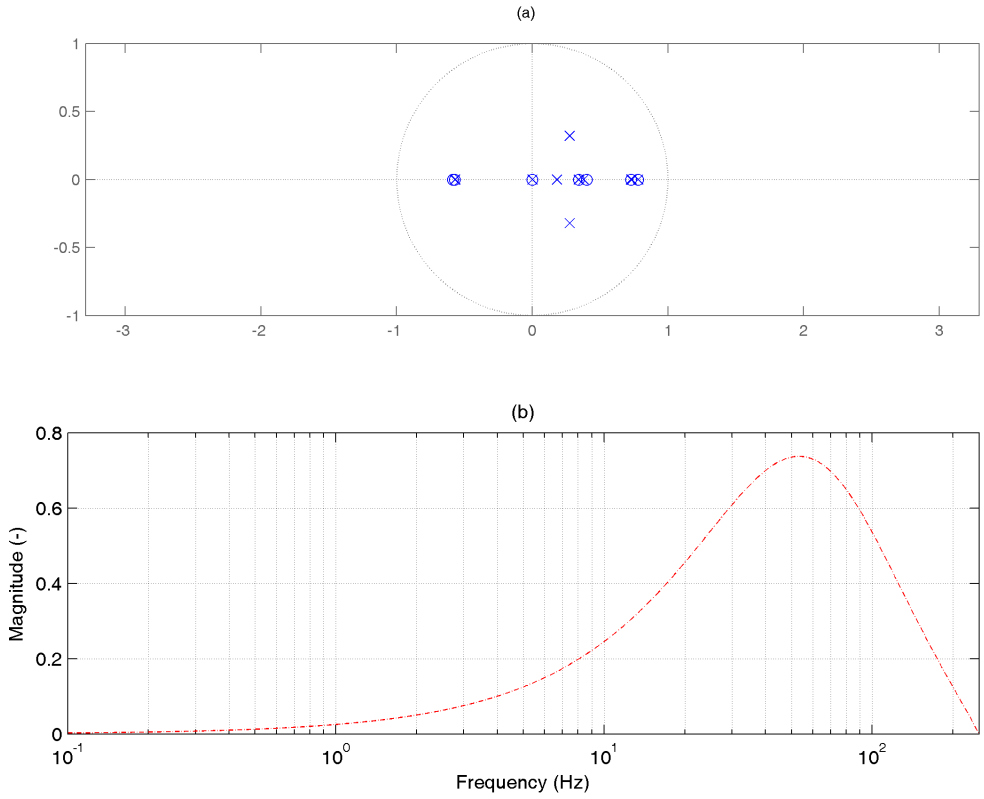

Figure 4.3 (a) The pole-zero map of our LQG controlled plant. (b) The regeneration spectrum of the RC for our LQG controlled plant.

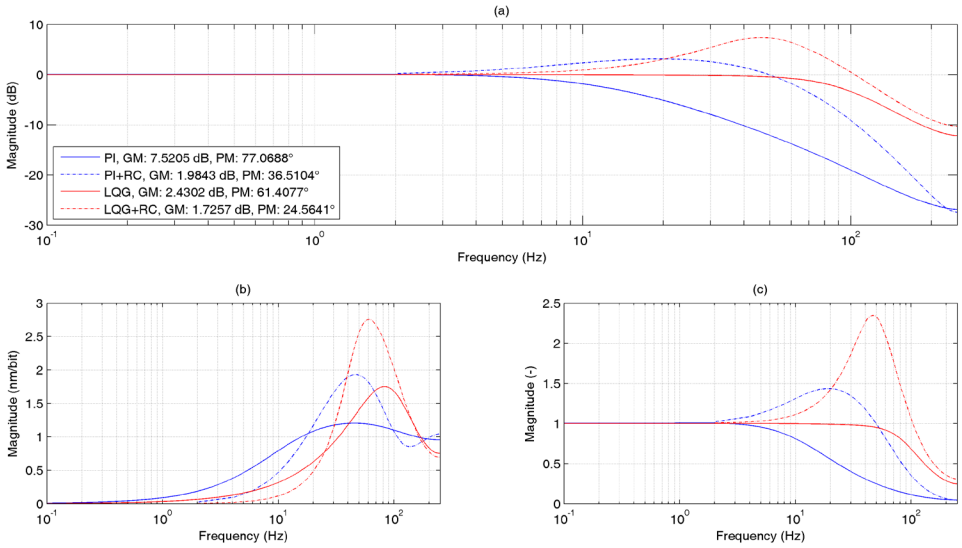

Figure 4.4 (a) The magnitude plots of the closed loop system under PI (solid blue line), PI+RC (dash-dotted blue line), LQG (solid red line) and LQG+RC (dash-dotted red line) controllers. (b) The sensitivity transfer function plots of the closed loop system under PI (solid blue line), PI+RC (dash-dotted blue line), LQG (solid red line) and LQG+RC (dash-dotted red line) controllers. (c) The complimentary sensitivity transfer function plots of the closed loop system under PI (solid blue line), PI+RC (dash-dotted blue line), LQG (solid red line) and LQG+RC (dash-dotted red line) controllers.

We then, investigate the performance and the robustness of all the controller schemes (PI, PI+RC, LQG, LQG+RC). The parameters of the PI+RC are also tuned by the Genetic Algorithms Toolbox of MATLAB, following the similar optimization procedure discussed in the previous chapter. To investigate the performance, we construct the magnitude plots of the closed loop system utilizing these four controllers. As shown in Figure 4.4a, the use of LQG controller extends the effective bandwidth of the plant compared to the traditional PI controlled systems at the expense of lower gain and phase

margins. This increase in bandwidth results in higher scan speeds. To investigate the robustness, we construct the sensitivity and the complementary sensitivity plots (Figs. 4.4b and 4.4c). The use of LQG controller reduces the effect of disturbance on the amplitude error significantly (Figure 4.4b) at low frequencies, but amplifies the effect of noise (Figure 4.4c) at high frequencies. One can also observe that the use of RC makes the system faster (see Figure 4.4a) but more sensitive to disturbance and measurement noise (compare the dash-dotted and solid lines in Figs. 4.4b and 4.4c). Moreover, the RC tends to push the feedback-only designs to the stability margins by further decreasing the gain and phase margins as can be observed in Figure 4.4a.

Finally, we analyze the sensitivity of the integrated scan error, IAE, to variations in optimal controller parameters obtained. We perturb the controller parameters R_w / R_v, Q / R and f_q by ±10%, and N_q, nb and nq by ±1 to investigate the percentage change in IAE. The results are tabulated in Table 4.1. As can be observed, the scan error is most sensitive to variations in N_q and nq, which are the two parameters related to the design of the filter q(z).

Table 4.1 Sensitivity of the scan error to variations in optimal controller parameters.

	R_w / R_v	Q / R	f_q	N_q	nb	nq
-10%, -1	0.0018	0.0029	0.1594	1.0987	0.0942	0.4651
+10%, +1	0.0016	0.0034	0.1545	0.8359	0.0210	0.9542

Chapter 5

RESULTS

To compare the performance of the LQG+RC to PI+RC, we have conducted scanning simulations in MATLAB/Simulink and physical experiments with our AFM setup at scan speeds of 3 μm/s (low) and 24 μm/s (high). The scanning simulations are performed with the surface shown in Figure 4.2.

This surface shows abrupt changes in height from 100 nm to 500 nm and vice versa. In our physical experiments, we use calibrated steps (MikroMasch, TGXYZ02), with a height of 100 nm and a pitch distance of 3 μm along the x-axis (Figure 1.1). In order to emulate the same abrupt changes in the surface profile, we perturb the control signal, z_{ref}, such that the step height abruptly changes from 100 nm to 500 nm after 30 lines are scanned along the y-axis (Figure 1.1) and then back to 100 nm abruptly after another 30 scan lines (30 lines correspond to 45 nm advancement along the y-axis).

The results of the scan simulations performed under PI+RC and LQG+RC at low and high scan speeds are shown in Figs. 5.1 and 5.2, respectively. The results suggest that

the IAE index is decreased by 42% (low) and 58% (high) when the LQG controller is used instead of the conventional PI controller.

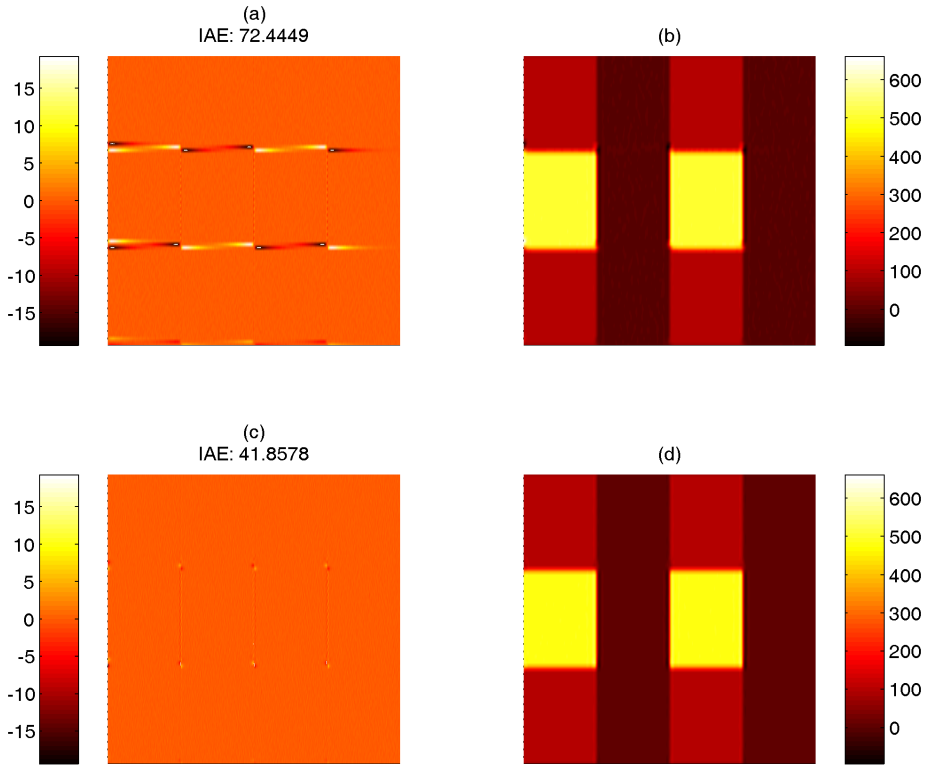

Figure 5.1 The results of the scanning simulations at low speed; the error and the surface profiles obtained under PI+RC (a, b) and LQG+RC (c, d).

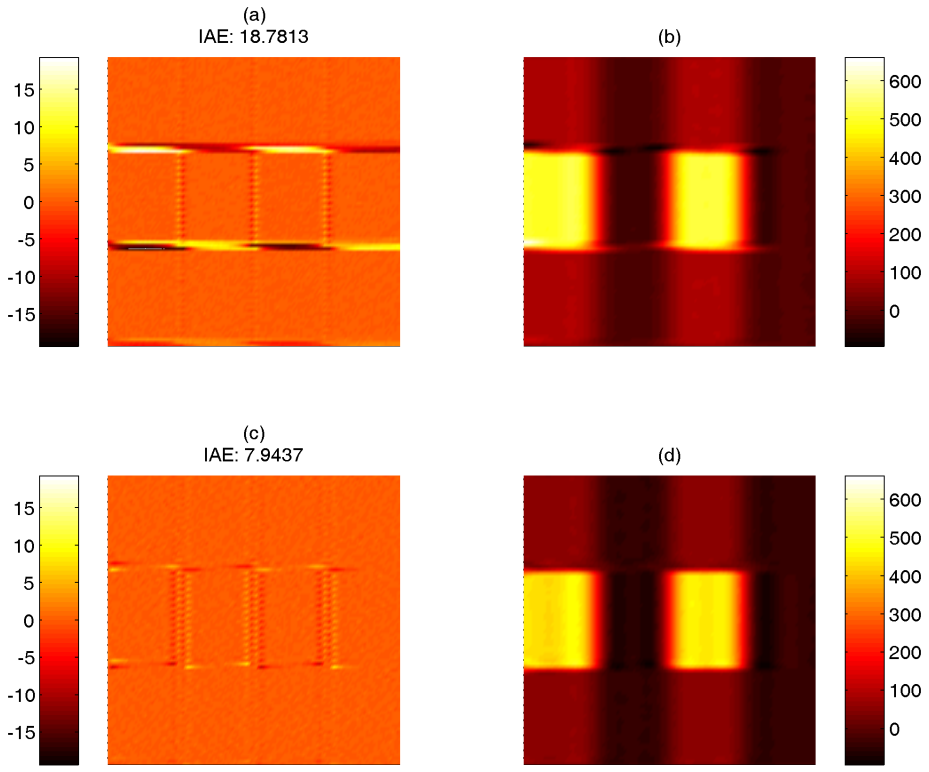

Figure 5.2 The results of the scanning simulations at high speed; the error and the surface profiles obtained under PI+RC (a, b) and LQG+RC (c, d).

When the same scans are performed in the physical world, we observe parallel results (see Figs. 5.3 and 5.4). The reduction in IAE index is now 54% and 45%, respectively. In both the simulations and the physical experiments, the scan images obtained under PI+RC are more distorted at high scan speeds.

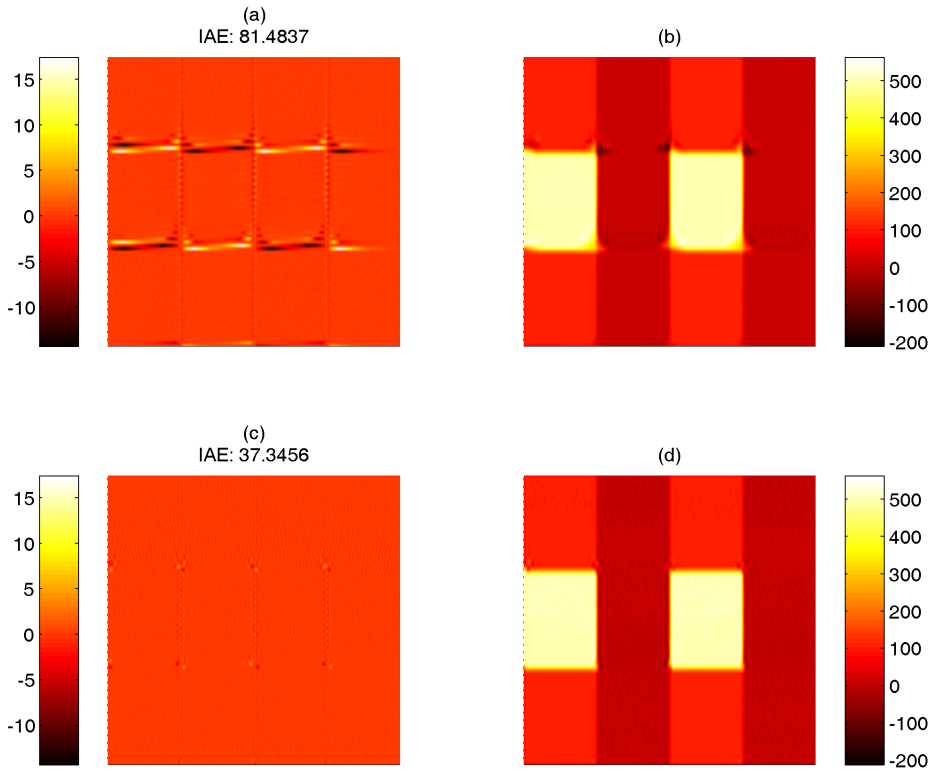

Figure 5.3 The results of the physical scanning experiments at low speed; the error and the surface profiles obtained under PI+RC (a, b) and LQG+RC (c, d).

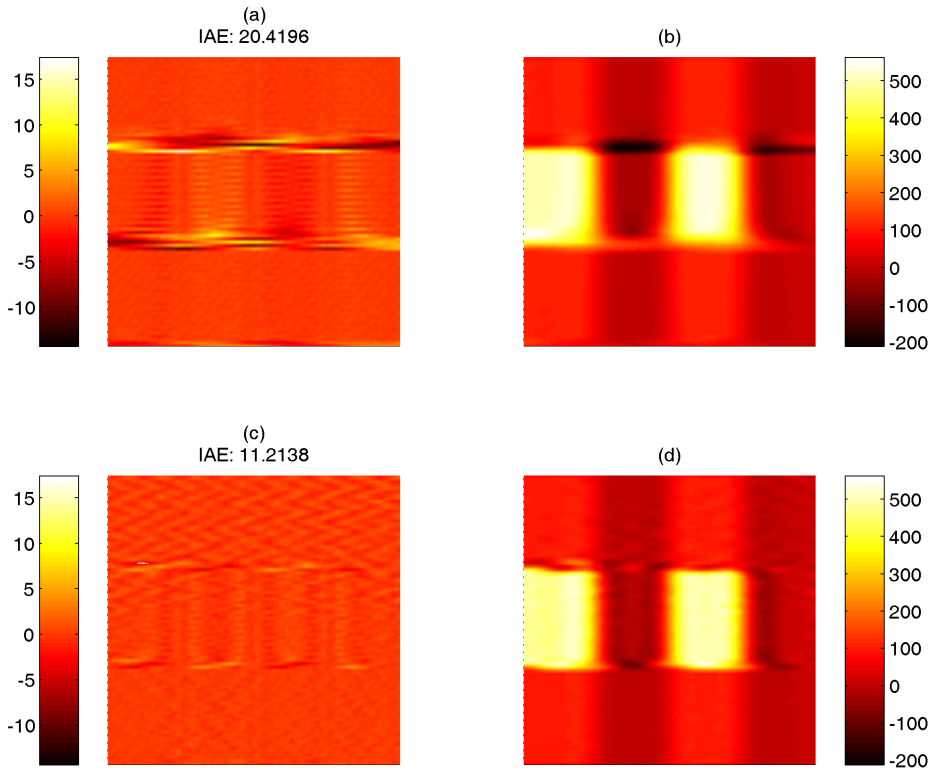

Figure 5.4 The results of the physical scanning experiments at high speed; the error and the surface profiles obtained under PI+RC (a, b) and LQG+RC (c, d).

Chapter 6

DISCUSSION

We have designed and implemented an LQG+RC controller for AFM scanning. The performance of the LQG+RC is superior to the performance of the PI+RC proposed in our earlier studies [16, 18]. The LQG controller is made of two parts: an optimal state estimator and a state feedback regulator. The first part enables us to estimate the states of the system and the second part enables us to design a full state feedback controller based on the estimated states. Since the designer can place the poles of the system to the optimal locations, this approach leads to higher scan rates than that of the conventional PI controller. In particular, the LQG controller improves the relatively slow dynamics of the tip-sample interactions (see Figure 3.2c). Moreover, since the effect of disturbance (i.e. surface profile) on the plant states can be observed instantaneously, a better control action can be taken in the short-term.

In order to provide a longer-term view for the controller, we take advantage of the repetitive nature of the scan lines and implement an RC. The RC memorizes the amplitude

error made in the previous scan loop and then adds to the one made in the current loop to augment the control action, which eventually eliminates the error (Figure 6.1).

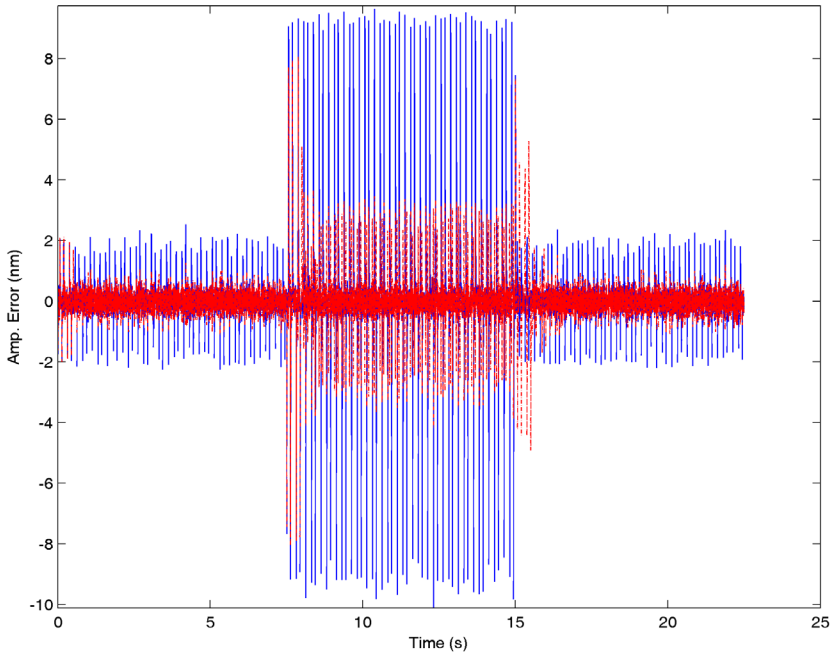

Figure 6.1 The amplitude error obtained under LQG (solid blue line) and LQG+RC (solid red line) controllers.

We show that the combined LQG+RC controller is not only faster than the PI+RC, but also handles surface variations of up to fivefold better. This is also confirmed by the sensitivity analysis. As shown in Figure 4.4b, the LQG+RC can suppress the effect of disturbance (i.e. abrupt changes in surface profile) on the vibration amplitude of probe better than the PI+RC in the range of our operating frequencies. The scan error under LQG+RC, quantified by the IAE index, is reduced by 45% (compared to PI+RC) when the

scanning speed is increased by eightfold. Since the interaction force between the probe tip and the surface is a function of the scan error [16], it can be argued that the probe tip and the surface are less likely to be damaged under the LQG+RC design.

It is important to note that there is a trade-off between disturbance suppression and noise cancelation in control systems. Hence, the LQG+RC is better at disturbance suppression in the range of our operating frequencies, it amplifies the measurement noise (Figure 4.4c), which shows itself in scan images, especially at high scan speeds (see the error profile in Figure 5.4c). Nevertheless, the adverse effect of noise on the scan images is reduced by using a low pass filter (see the scan profile in Figure 5.4d).

A comprehensive MATLAB/Simulink model (Figure 2.1) has been developed to simulate the whole scan process and test the performance of the proposed LQG+RC under different settings. Our simulation results show strong agreement with those of the physical experiments performed in our AFM setup. Since the scan performance in a physical set-up depends on many factors (such as temperature, humidity, ground vibrations, electrical and environmental noise, etc.), which are not under the full control of an experimenter, testing the performance of a new controller in a simulation environment under different settings is highly beneficial. More importantly, the simulation model enables us to calculate the optimal values of the control parameters used for the physical experiments. Without the simulation model and the use of genetic algorithms, the selection of the control parameters in our design would be highly challenging.

Chapter 7

CONCLUSION

A combination of various feedback and feedforward controllers has been suggested for AFM systems to increase the scan speed and image quality. However, we are not aware of an earlier study utilizing LQG+RC controller for AFM scanning. The LQG controller can observe and regulate all states of the plant and hence improves the transient response of the RC better than the PI controller. Nevertheless, this requires a linear and an accurate model of the plant. In the implementation of the LQG controller, we assumed constant values for the state and the measurement noises and then calculated all the controller gains off-line accordingly. However, if these noise levels are subject to variations, as it may happen in AFM systems, the controller gains must be updated online by solving the Riccati equations, which brings additional computational load to the controller.

BIBLIOGRAPHY

[1] K. K. Leang and S. Devasia, "Hysteresis, creep, and vibration compensation for piezoactuators: Feedback and feedforward control," in The 2nd IFAC Conference on Mechatronic Systems, 2002, pp. 283-289.

[2] S. Devasia, E. Eleftheriou, and S. O. R. Moheimani, "A survey of control issues in nanopositioning," IEEE Transactions on Control Systems Technology, vol. 15, pp. 802-823, Sep 2007.

[3] G. M. Clayton, S. Tien, K. K. Leang, Q. Z. Zou, and S. Devasia, "A Review of Feedforward Control Approaches in Nanopositioning for High-Speed SPM," Journal of Dynamic Systems Measurement and Control-Transactions of the ASME, vol. 131, Nov 2009.

[4] D. Y. Abramovitch, S. Hoen, and R. Workman, "Semi-Automatic Tuning of Pid Gains for Atomic Force Microscopes," Asian Journal of Control, vol. 11, pp. 188-195, Mar 2009.

[5] G. Schitter, P. Menold, H. F. Knapp, F. Allgower, and A. Stemmer, "High performance feedback for fast scanning atomic force microscopes," Review of Scientific Instruments, vol. 72, pp. 3320-3327, Aug 2001.

[6] S. Salapaka, A. Sebastian, J. P. Cleveland, and M. V. Salapaka, "High bandwidth nano-positioner: A robust control approach," Review of Scientific Instruments, vol. 73, pp. 3232-3241, Sep 2002.

[7] G. Schitter, R. W. Stark, and A. Stemmer, "Fast feedback control of piezoelectric actuators," in 8th Int. Conf. on New Actuators, Bremen, Germany, 2002, pp. pp. 430-433.

[8] A. Sebastian and S. M. Salapaka, "Design methodologies for robust nano-positioning," IEEE Transactions on Control Systems Technology, vol. 13, pp. 868-876, Nov 2005.

[9] C. J. Lin and S. R. Yang, "Precise positioning of piezo-actuated stages using hysteresis-observer based control," Mechatronics, vol. 16, pp. 417-426, Sep 2006.

[10] K. K. Leang and S. Devasia, "Feedback-linearized inverse feedforward for creep, hysteresis, and vibration compensation in AFM piezoactuators," IEEE Transactions on Control Systems Technology, vol. 15, pp. 927-935, Sep 2007.

[11] G. Schitter, R. W. Stark, and A. Stemmer, "Fast contact-mode atomic force microscopy on biological specimen by model-based control," Ultramicroscopy, vol. 100, pp. 253-257, Aug 2004.

[12] T. Shiraishi and H. Fujimoto, "High-speed High-precision Control of Atomic Force Microscope by Surface Topography Learning Observer," in American Control Conference, 2009, pp. 961-966.

[13] Y. Wu, Q. Z. Zou, and C. M. Su, "A Current Cycle Feedback Iterative Learning Control Approach for AFM Imaging," IEEE Transactions on Nanotechnology, vol. 8, pp. 515-527, Jul 2009.

[14] B. E. Helfrich, C. Lee, D. A. Bristow, X. H. Xiao, J. Y. Dong, A. G. Alleyne, et al., "Combined H-infinity-Feedback Control and Iterative Learning Control Design With Application to Nanopositioning Systems," IEEE Transactions on Control Systems Technology, vol. 18, pp. 336-351, Mar 2010.

[15] U. Aridogan, Y. F. Shan, and K. K. Leang, "Design and Analysis of Discrete-Time Repetitive Control for Scanning Probe Microscopes," Journal of Dynamic Systems Measurement and Control-Transactions of the ASME, vol. 131, Nov 2009.

[16] S. Necipoglu, S. A. Cebeci, Y. E. Has, L. Guvenc, and C. Basdogan, "Robust Repetitive Controller for Fast AFM Imaging," IEEE Transactions on Nanotechnology, vol. 10, pp. 1074-1082, Sep 2011.

[17] R. J. E. Merry, M. J. C. Ronde, R. van de Molengraft, K. R. Koops, and M. Steinbuch, "Directional Repetitive Control of a Metrological AFM," IEEE Transactions on Control Systems Technology, vol. 19, pp. 1622-1629, Nov 2011.

[18] S. Necipoglu, S. A. Cebeci, C. Basdogan, Y. E. Has, and L. Guvenc, "Repetitive control of an XYZ piezo-stage for faster nano-scanning: Numerical simulations and experiments," Mechatronics, vol. 21, pp. 1098-1107, Sep 2011.

[19] H. R. Habibullah and I. R. Petersen, "LQG Controller with a Vibration Compensator for the Lateral Positioning of an AFM Scanner," in Australian Control Conference, 2012, pp. 324-329.

[20] I. Gunev, A. Varol, S. Karaman, and C. Basdogan, "Adaptive Q control for tapping-mode nanoscanning using a piezoactuated bimorph probe," Review of Scientific Instruments, vol. 78, Apr 2007.

[21] K. J. Astrom and B. Wittenmark, Computer-Controlled Systems: Theory and Design, 3 ed.: Prentice Hall, 1996.

[22] H. Kwakernaak and R. Sivan, Linear Optimal Control Systems Wiley-Interscience, 1972.